Concentration profiles of colloidal mixtures in a cylindrical pore

M. Chávez-Páez, E. Urrutia-Bañuelos, and M. Medina-Noyola
Instituto de Física ''Manuel Sandoval Vallarta,'' Universidad Autónoma de San Luis Potosí, Apartado Postal 629, 78000 San Luis Potosí, SLP, Mexico
(Received 24 November 1997)

The concentration profiles of a model colloidal mixture inside a charged cylindrical pore are studied theoretically and by computer simulations. The theoretical structure of the colloidal mixture is obtained by employing the basic chemical equilibrium equations from which the concentration profiles can be expressed in terms of a set of integral equations. The pair potential between particles is taken to be the repulsive part of the Derjaguin-Landau-Verwey-Overbeek potential. Simulation results are also presented in order to assess the accuracy of the theoretical predictions. [S1063-651X(98)12506-0]

PACS number(s): 82.70.Dd, 05.40.+j

I. INTRODUCTION

The determination of the structure of colloidal suspensions has been an active area of research through the last years. This area of research has benefited from the application of modern experimental techniques, such as light and neutron scattering, on rather clean and well characterized model experimental systems. As a result, the experimentally determined static structure factors in these systems have been compared quite successfully with the predictions of fairly simple theoretical models and approximations. Thus, for example, we can say that the basic features of the static structure of dilute aqueous suspensions of highly charged particles in the bulk are well understood on the basis of the Derjaguin-Landau-Verwey-Overbeek (DLVO) model for the pair interactions [1].

On the other hand, the recently reported attempts to directly measure the interaction forces between colloidal particles near a charged surface [2,3], and the structure of the suspension that these forces induce in the vicinity of such a surface, have prompted the proposal of theoretical models and approximations to describe the structure of a monodisperse suspension of highly charged colloidal particles near charged walls [4–6]. These developments were based on the DLVO level of description of the particle-particle and wall-particle interactions, and on the use of simple, but well-established, approximations borrowed from the equilibrium theory of inhomogeneous liquids. Within the same spirit, the structure of suspensions of highly charged particles confined in the interior of charged cylinders has also been studied [7]. In such work the concentration profile of a monodisperse charged colloidal suspension inside a charged cylindrical pore has been calculated, and interesting effects were observed. Thus, for example, it was found that for the limiting case of very thick cylinders, the concentration profile $n(\rho)$ approaches the structure of a suspension in front of a flat wall, and becomes independent of the size of the cylinder, and also independent of the strength of the wall-particle repulsion. These scaling properties were also found to hold approximately for the main peak of the concentration profile even in the opposite limit of very narrow cylinders.

Along this line of research, in this paper we report the results of our recent work on the description of a model colloidal binary mixture that permeates a cylindrical pore. Thus, here we calculate the concentration profiles $n_i(\mathbf{r})$, $i=1,2$, of the two species of a colloidal mixture in the interior of a pore, which is in contact with a reservoir at bulk concentrations n_1 and n_2. The theoretical calculations derive from a straightforward extension of the scheme employed before in the context of monodisperse suspensions [7]. This approximate theory allows us to calculate the concentration profiles $n_i(\mathbf{r})$ for a variety of conditions, and the accuracy of the theoretical predictions can be tested by comparing with computer simulations. We perform Brownian dynamics simulations for some of the systems we study and the comparison is reported. Such comparison indicates that the theoretical scheme provides the correct general picture of this structural property. In Sec. II we explain the model system studied, and present the approximate theory employed to calculate $n_i(\mathbf{r})$. In addition, we give some details of the computer simulations. The results are presented and discussed in Sec. III. The main conclusions are summarized in Sec. IV.

II. THEORETICAL APPROACH AND COMPUTER SIMULATIONS

Consider a colloidal mixture of highly charged spheres in water at low ionic strength, and imagine that we have a very long capillary of inner radius R immersed in the suspension. Our aim is to determine the concentration profiles (i.e., the equilibrium average local concentration) of the suspended particles at any point in the interior of this capillary. Given the symmetry of the system, the density profiles depend only on the distance ρ to the cylinder's axis, i.e., $n_i(\mathbf{r})=n_i(\rho)$, with $i=1,2$, and on the elementary parameters defining the system. These are those pertaining to the suspension [the diameter σ_i and charge Q_i of the particles of species $i=1,2$, the molar fractions $x_i=n_i/(n_1+n_2)$, the total bulk concentration $n=n_1+n_2$, and the inverse Debye length κ], and those referring to the capillary (the radius R, and the inner surface charge density σ_{el}). Rather than stressing the detailed manner in which the interaction forces depend on each of these parameters, we consider instead an idealized model, and will study the structure of such a model colloidal mix-

ture in which the elementary parameters are contracted into a few effective parameters appearing in the particle-particle and wall-particle interaction potentials. Thus, we shall model the interaction potential of two particles, one of species i and another of species j, separated by a distance r, by the screened Coulomb or Yukawa potential, written as [1]

$$\beta u_{ij}(r)=\begin{cases}\infty, & r<\sigma\\ K_iK_j\dfrac{\exp[-z_D(r/\sigma-1)]}{(r/\sigma)}, & r>\sigma,\end{cases} \tag{2.1}$$

where we assume the particles to have the same hard-sphere diameter σ. Here, $\beta^{-1}=k_BT$, with k_B being Boltzmann's constant and T the temperature, and $z_D\equiv\kappa\sigma$ with κ being the inverse Debye length. Thus, K_iK_j is the contact potential between two particles of species i and j in units of k_BT.

As for the potential $\Psi_i(\mathbf{r})$ of the force exerted by the charge density of the cylinder's inner surface on a particle of charge Q_i at position $\mathbf{r}$ inside the cylinder we will use the form [7]

$$\beta\Psi_i(\rho)=K_iK_w\frac{I_0(\kappa\rho)}{I_0(\kappa R')-1}, \quad \rho<R', \tag{2.2}$$

where $I_0(x)$ is the modified Bessel function of order zero [8], and R' is the distance from the cylinder axis to the point at which a particle is in hard contact with the cylinder's inner wall. Thus, if R is the actual radius of the cylinder, then $R'\equiv R-\sigma/2$. From Eq. (2.2) we have that K_iK_w is the electrostatic potential energy, in units of k_BT, of a particle of species i in contact with the cylinder wall, referring to the potential at the cylinder's axis. We can expect that K_i is linear in Q_i, and K_w is linear in $\sigma_{\rm el}$, so that variations in K_w, for example, are equivalent to variations in $\sigma_{\rm el}$.

Let us suppose that the confined suspension is in equilibrium with a homogeneous system of uniform densities n_1 and n_2, temperature T, and chemical potentials μ_1 and μ_2. To determine the equilibrium local particle concentration $n_i(\mathbf{r})$ $(i=1,2)$, which corresponds to the external potential $\Psi_i(\mathbf{r})$, we solve the following coupled equations [7,9]:

$$\ln\left[\frac{n_i(\mathbf{r})}{n_i}\right]+\beta\Psi_i(\mathbf{r})=\sum_{j=1}^{2}\int d^3r'c_{ij}^b(|\mathbf{r}-\mathbf{r}'|)[n_j(\mathbf{r}')-n_j]. \tag{2.3}$$

Here $c_{ij}^b(r)$ is the bulk particle-particle direct correlation function between particles of species i and j, respectively. This function is formally defined through the Ornstein-Zernike equations

$$h_{ij}^b(r)=c_{ij}^b(r)+\sum_{k=1}^{2}n_k\int d^3r'h_{ik}^b(r')c_{kj}^b(|\mathbf{r}-\mathbf{r}'|), \tag{2.4}$$

where $h_{ij}^b(r)$ is the total bulk correlation function of species i and j. To determine $c_{ij}^b(r)$ it is necessary to provide a further relation between $h_{ij}^b(r)$ and $c_{ij}^b(r)$. In this work we use the Rogers-Young closure relation [10], which reads

$$c_{ij}^b(r)=e^{-\beta u_{ij}(r)}\left[1+\frac{e^{\gamma_{ij}^b(r)f(r)}}{f(r)}\right]-\gamma_{ij}^b(r)-1, \tag{2.5}$$

where $\gamma_{ij}^b(r)=h_{ij}^b(r)-c_{ij}^b(r)$ is the so-called indirect correlation function, and $f(r)=1-\exp(-\alpha r)$. Equations (2.4) and (2.5) are solved iteratively, using α as an adjustable parameter to satisfy partial thermodynamic consistency. This closure relation, Eq. (2.5), has proved to be highly accurate in predicting the structure of the bulk Yukawa fluid [11].

Due to the symmetry of the external potential the concentration profiles $n_i(\mathbf{r})$ only depend on the distance ρ from the center of the cylinder. Thus, Eqs. (2.3) can be rewritten as

$$\ln[1+H_i(\rho)]+\beta\Psi_i(\rho)=\sum_{j=1}^{2}n_j\int d^3r'c_{ij}^b(|\mathbf{r}-\mathbf{r}'|)H_j(\rho'). \tag{2.6}$$

In this case $H_i(\rho)$ is defined in terms of the concentration profile $n_i(\rho)$ through the relation

$$H_i(\rho)=\frac{n_i(\rho)}{n_i}-1. \tag{2.7}$$

To assess the predictions of this simple theoretical scheme we have carried out Brownian dynamics simulations to calculate the concentration profile of the particles inside the cylinder and, in order to minimize edge effects due to the finite size of the simulation system, conventional [12] periodic boundary conditions in the z direction are used. The method of Brownian dynamics, as proposed by Ermak and McCammon [13], is based on the solution of the generalized N-particle diffusion equation. Within this scheme, the displacement of the ith particle (during a short enough time interval Δt) is given by

$$\mathbf{r}_i(t+\Delta t)-\mathbf{r}_i(t)=\beta D_0\mathbf{F}_i\Delta t+\mathbf{R}_i(\Delta t), \tag{2.8}$$

where D_0 is the free-particle diffusion coefficient, and $\mathbf{R}_i(\Delta t)$ is a random Gaussian displacement of the particle, which is assumed to have zero mean and variance $6D_0\Delta t$. The force $\mathbf{F}_i$ in this equation arises from the direct interactions of the ith particle with the cylinder's field of force and with the other Brownian particles in the system. It should be noticed, however, that in this paper we only report equilibrium properties, which are independent of the particular dynamic algorithm employed in these simulations.

The connection of the computer simulations with the theoretical results is made by fixing the number of particles N_1 and N_2 inside the volume πR^2L of the basic simulation cell (of length L in the z direction) such that

$$\frac{N_i}{\pi R^2L}=\frac{2}{R^2}\int_0^R n_i(\rho)\rho d\rho\equiv\overline{n_i}, \tag{2.9}$$

where $n_i(\rho)$ is obtained from the solution of Eqs. (2.6) and (2.7). Thus, Eq. (2.9) defines the corresponding mean concentration of species i, $\overline{n_i}$, inside the cylinder.

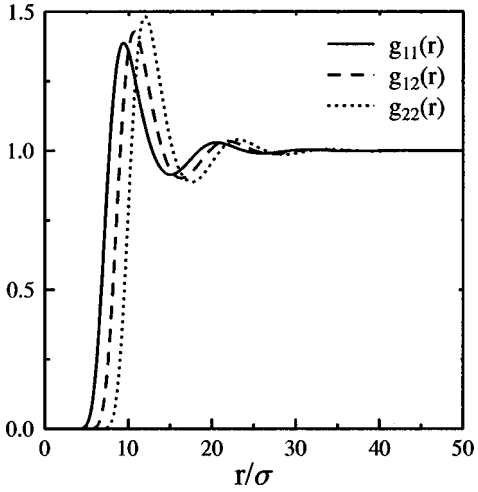

FIG. 1. Theoretical pair correlation functions for a colloidal mixture in the bulk regime. Particles follow the pair interaction given by Eq. (2.1). The parameters in the system are $K_1=10$, $K_2=20$, $z_D=0.15$, $x_1=0.5$, and $n^*=8.4\times10^{-4}$.

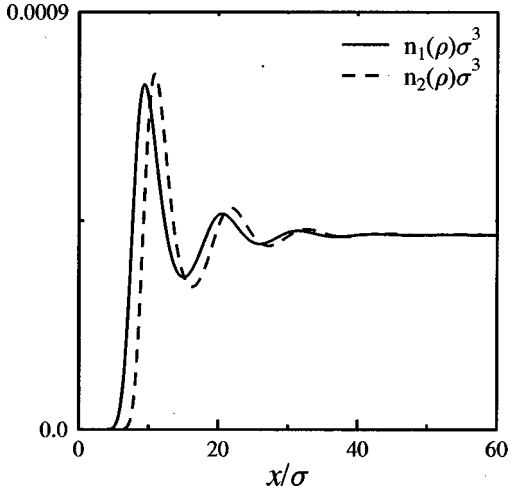

FIG. 2. Theoretical concentration profiles $n_1^*(\rho)$ and $n_2^*(\rho)$, plotted as a function of the distance from the wall $x=R'-\rho$. The bulk parameters are $K_1=10$, $K_2=20$, $z_D=0.15$, $x_1=0.5$, and $n^*=8.4\times10^{-4}$. The cylinder parameters are $K_w=10$ and $R'=100\sigma$.

III. RESULTS

In what follows, we first report the results for $n_i(\rho)$ obtained from the approximate theoretical scheme defined above. This will allow us to explain the main features of this structural property in the regimes that we refer to as ''thick'' and ''narrow'' cylinders. As it turns out, the features and trends predicted by the theoretical results are also observed in the computer-simulated results. The quantitative comparison of the theoretical and simulated results will be presented at the end of this section.

Let us present the results for the density profiles $n_i^*(\rho)\equiv n^*x_i[1+H_i(\rho)]$, where n^* is the dimensionless bulk number concentration $n^*=n\sigma^3$ and $x_i=n_i/n$ is the molar fraction of species i. Among all the possible values of the parameters of the system we could consider, we will choose them appropriately to illustrate the regimes appearing when the weakly screened electrostatic interactions dominate. In particular, in this work we will consider a bulk system with parameters $z_D=0.15$, $x_1=0.5$, $K_1=10$, $K_2=20$, and $n^*=8.4\times10^{-4}$, whose bulk structure is represented by the radial distribution functions $g_{11}(r), g_{12}(r), g_{22}(r)$ (see Fig. 1), and whose relevant length scales are the mean interparticle distance $\ell^*=\ell/\sigma\equiv n^{*-1/3}(=10.6)$, the screening length $z_D^{-1}(=6.67)$, and the correlation length $\lambda^*=\lambda/\sigma(\sim4\ell^*)$, i.e., the distance at which the radial distribution functions reach their asymptotic values. With this bulk system as a reservoir, let us consider the structure of the suspension inside a highly charged cylinder such that the hard contact between the particles and the wall is completely unlikely (i.e., $K_w\gg1$). In this manner, $n_i(\rho)$ $(i=1, 2)$ will be nearly zero not only at wall-particle contact, but also within a finite region between the wall $(\rho=R')$ and a certain distance d of closest approach to the wall, which defines an effective radius $R_{\rm ef}=R'-d$ of the cylinder.

A. Thick cylinders

The first case we consider corresponds to the regime of thick cylinders, i.e., the regime in which the particles are confined to a region of the order of, or larger than, the correlation length (i.e., $R_{\rm ef}\gtrsim\lambda$). Figure 2 shows the concentration profiles $n_1^*(\rho)$ and $n_2^*(\rho)$ as obtained from the solution of the theory for the illustrative bulk parameters mentioned above $(K_1=10, K_2=20, z_D=0.15, x_1=0.5, n^*=8.4\times10^{-4})$ and for $K_w=10$, and $R'=100\sigma$. The curves are plotted as a function of the distance from the wall, $x\equiv R'-\rho$. This figure illustrates the general behavior of the concentration profiles. Thus, for example, the figure shows the appearance of depletion gaps next to the wall where no particles are allowed to be in. One can notice that the gap corresponding to the more charged species (species 2) is larger than the gap corresponding to species 1 (a feature that is shared by all the systems studied here). The origin of this effect is the higher wall-particle repulsion experienced by particles of species 2 as compared to species 1. Beyond these depletion gaps, the concentration profiles present a series of peaks whose height decreases with the distance from the wall, until the concentration profiles reach their asymptotic value n_1 and n_2, respectively. The appearance of bulklike regions around the center of the cylinder (the region $x>40\sigma$ in Fig. 2) illustrates the loss of wall-particle correlations.

In order to show the differences arising from the reduction of the space available to the particles, in Fig. 3(a) we compare the results corresponding to the case $R'=50\sigma$ (still $R_{\rm ef}\gtrsim\lambda$) along with the previous case $R'=100\sigma$. In this figure the width of the depletion gaps and the position of the peaks of the two systems remain virtually the same, although the heights of the peaks are slightly increased. This indicates that the width of the depletion gaps and the position of the peaks are independent of R' in the regime of very thick cylinders. Moreover, we have found (not shown here) that for $R'>70\sigma$ the structure calculated for two different radii is identical to the structure already shown in Fig. 2. This means that for the parameters employed here, $R'=70\sigma$ constitutes the threshold of the regime of very thick cylinders, characterized by the appearance of well-defined bulklike regions in the middle of the cylinder and by the independence of the concentration profiles on the cylinder's radius R. We can see

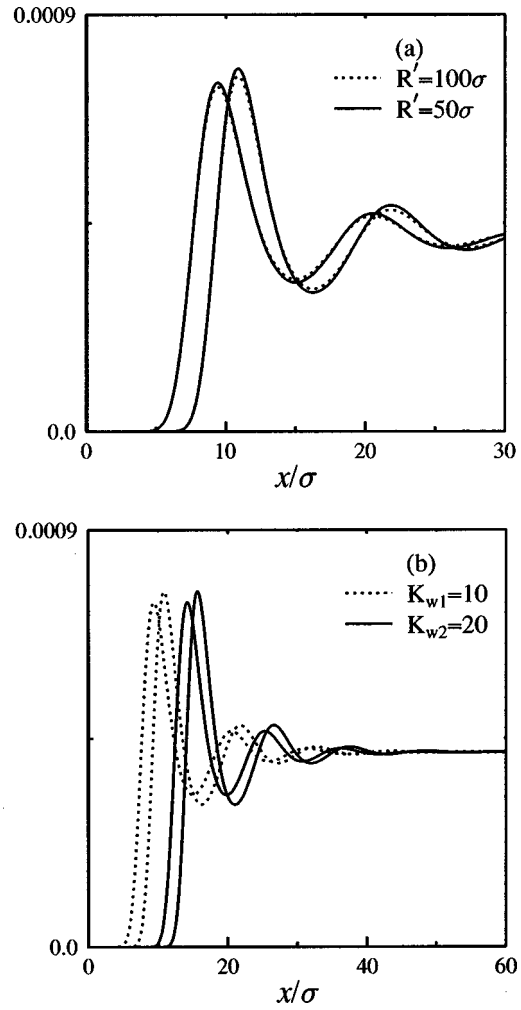

FIG. 3. (a) Theoretical concentration profiles for two different values of R' $(=100\sigma,50\sigma)$, plotted as a function of $x=R'-\rho$. Solid lines stand for $R'=50\sigma$ and dotted lines stand for $R'=100\sigma$. In both cases, the curve closest to the wall corresponds to $n_1^*(\rho)$. The rest of the parameters are as in Fig. 2. (b) Theoretical concentration profiles for $R'=100\sigma$ and for two different values of K_w $(=10,20)$, plotted as a function of $x=R'-\rho$. The bulk parameters are as in Fig. 2. The solid curves correspond to $n_1^*(\rho)$ and $n_2^*(\rho)$ for $K_w=20$, and the dotted curves correspond to $K_w=10$. In both cases, the curve closest to the wall corresponds to $n_1^*(\rho)$.

that these features derive from the asymptotic behavior of the wall-particle potential, since in the limit of large R' the wall-particle potential (2.2), as a function of $x=R'-\rho$, takes the form

$$\beta\Psi_i(x=R'-\rho)\approx K_iK_w\exp(-\kappa x), \tag{3.1}$$

which does not depend on R'.

Due to this asymptotic form of the wall-particle interaction, a second scaling property of the structure of the suspension inside thick cylinders can be inferred. From Eq. (3.1) we have that for two cylinders connected to the same reservoir, but one characterized by R_1 and K_{w1}, and the other by R_2 and K_{w2}, the following relation holds

$$\beta\Psi_i(\rho,R_1,K_{w1},K_i)=\beta\Psi_i(\rho,R_2,K_{w2},K_i) \tag{3.2}$$

provided that

$$R_2=R_1+\kappa^{-1}\ln(K_{w2}/K_{w1}). \tag{3.3}$$

Taking into account that in this limit the structure does not depend on R', we have that the concentration profiles for two different values of K_w are identical, when plotted as a function of the distance from the wall, except for a shift given by

$$\delta=\kappa^{-1}\ln(K_{w2}/K_{w1}). \tag{3.4}$$

This effect is illustrated in Fig. 3(b), where we have plotted the concentration profiles for two different systems, one characterized by $K_{w1}=10$ and the other by $K_{w2}=20$, for the same radius of the cylinder $R_1=R_2=100\sigma$. As it happens, if the curves corresponding to $K_{w2}=20$ are shifted to the left by $\delta=\kappa^{-1}\ln(K_{w2}/K_{w1})=4.62\sigma$, they will superimpose on the curves corresponding to $K_{w1}=10$. Taking into account the results presented in Figs. 3(a) and 3(b), we can say that, in the limit of very thick cylinders, and for a given system in the bulk (i.e., given bulk density, molar composition, and interaction parameters of the colloidal suspension), the width of the depletion gaps only depends on K_w, but not on the thickness R of the cylinder.

We can summarize the results presented up to this point by stating that in the regime of very thick cylinders, where a bulklike region in the middle of the cylinder appears, the shape of the concentration profiles are independent on both the size (i.e., the radius) of the cylinder and the strength of the wall-particle repulsion, up to a shift given by Eq. (3.4).

B. Narrow cylinders

Let us now consider the regime in which the particles are confined to a region of the order of the correlation length λ or smaller, i.e., $R_{ef}\lesssim\lambda$. Our aim now is to show the effects on the structure due to variations in the wall-particle interactions. Before we do this, let us first show the deviations arising from the reduction of the cylinder's size in going from the limiting case of very thick, to narrow cylinders. This is done in Fig. 4 where we have replotted the curves of the system already presented in Fig. 2 $(R'=100\sigma)$, along with a system with the same parameters but with $R'=30\sigma$. The comparison of the two regimes indicates that the reduction of the cylinder's size emphasizes the wall-particle correlations, as indicated by the rise in the height of the peaks, although their positions remain almost the same. Thus, we can conclude that in both regimes, very thick and narrow cylinders, the positions of the main peaks are only weakly dependent of the size of the cylinder, and the effect of reducing the radius only emphasizes slightly the structure of the confined suspension.

Once we have presented the effects induced by the reduction of the cylinder's size, let us now consider the evolution of the structure when the wall-particle interaction varies. This is done in Fig. 5(a), where the concentration profiles in the interior of narrow cylinders $(R'=30\sigma)$ are plotted for two different values of K_w $(=5,10)$. One feature to notice is that, as in the case of very thick cylinders, particles of species 2 are always further away from the wall than particles of species 1. On the other hand, the structure becomes more

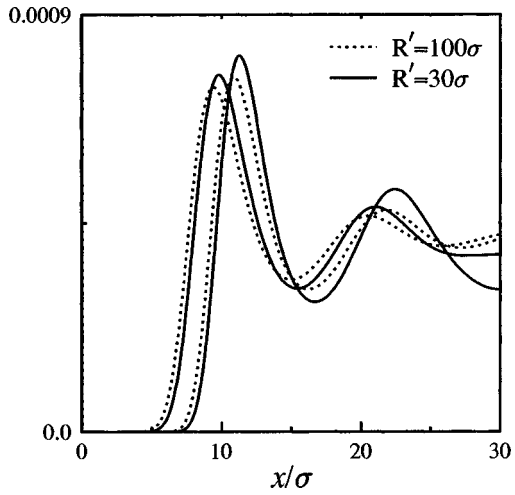

FIG. 4. Theoretical concentration profiles for $K_w=10$ and for two different values of R' $(=30\sigma,100\sigma)$. The curves are plotted as a function of the distance from the wall, $x=R'-\rho$. The bulk parameters are as in Fig. 2. The solid curves correspond to $n_1^*(\rho)$ and $n_2^*(\rho)$ for $R'=30\sigma$, and the dotted curves correspond to $R'=100\sigma$. In both cases, the curve closest to the wall corresponds to $n_1^*(\rho)$.

confined when the interaction with the wall increases, as shown in Fig. 5(a). For example, for $K_w=5$, the concentration profiles become nonzero near the wall ($d\approx 0$ for species 1 and $d\approx 2.5\sigma$ for species 2) and both species present three peaks in their concentration profiles, whereas for $K_w=10$ the concentration profiles becomes nonzero still further from the wall ($d\approx 6\sigma$ for species 1 and $d\approx 7.5\sigma$ for species 2), and both species present only two peaks in their concentration profiles.

As we saw in the case of thick cylinders the concentration profiles for a given value of the radius R' and for different values of K_w are identical, up to a shift given by Eq. (3.4). It is interesting to see to what extent this scaling property is still satisfied in the regime of narrow cylinders, since in this case the first peak (the peak closest to the wall) of both $n_1^*(\rho)$ and $n_2^*(\rho)$ shifts to the center of the cylinder when K_w increases, but their shape remains almost the same, as shown in Fig. 5(a). In order to illustrate this feature, in Fig. 5(b) we plot the same systems presented in Fig. 5(a), but with the two curves corresponding to $K_w=10$ shifted to the left in such a way that the maximum of the first peak of $n_1^*(\rho)$ coincides with the maximum of the first peak of $n_1^*(\rho)$ for the case $K_w=5$. In can be appreciated that the superposition of the curves is still quite good, and even the second peaks are very similar. This feature is reminiscent of the scaling properties of very thick cylinders discussed above, although in this case the shift is not quantitatively given by Eq. (3.4).

C. Comparison with computer simulations

Let us now present the comparison of the theoretical predictions with computer simulations. For such a comparison, let us consider a system with parameters $K_w=10$, and $R'=30\sigma$ (and the originally fixed values $K_1=10$, $K_2=20$, $z_D=0.15$, $n^*=8.4\times 10^{-4}$, and $x_1=x_2=0.5$). For these parameters, the theoretical results for the mean concentration of

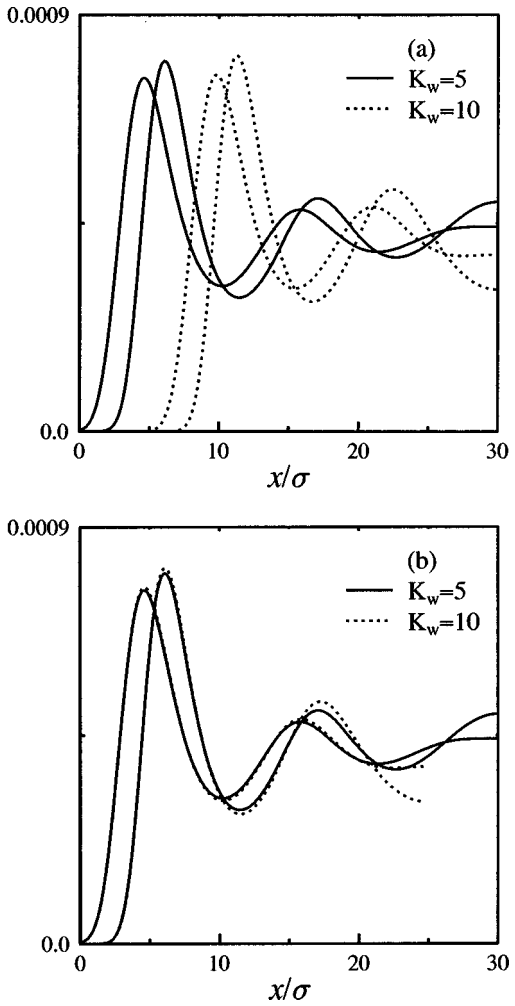

FIG. 5. (a) Theoretical concentration profiles for two different values of K_w $(=5,10)$ and for $R'=30\sigma$. The curves are plotted as a function of the distance from the wall, $x=R'-\rho$. The rest of the parameters are $K_1=10$, $K_2=20$, $z_D=0.15$, $x_1=0.5$, and $n^*=8.4\times 10^{-4}$. The solid curves correspond to $n_1^*(\rho)$ and $n_2^*(\rho)$ for $K_w=5$, and the dotted curves correspond to $K_w=10$. In both cases, the curve closest to the wall corresponds to $n_1^*(\rho)$. (b) The same as in (a), but the two curves corresponding to $K_w=10$ are shifted in such a way that the position of the first maximum of $n_1^*(\rho)$ coincides with the position of the first maximum of the calculated $n_1^*(\rho)$ for $K_w=5$.

particles inside the cylinder are $\bar{n}_1^*\equiv\bar{n}_1\sigma^3=2.69\times 10^{-4}$ and $\bar{n}_2^*\equiv\bar{n}_2\sigma^3=2.32\times 10^{-4}$. As explained before, these values of $\bar{n}_1^*$ and $\bar{n}_2^*$ are employed in the computer simulations, and the corresponding concentration profiles are plotted in Fig. 6(a), as a function of the distance x from the wall. We see from this figure that the qualitative agreement between theory and simulations is good, at least with respect to the position and number of peaks, and this degree of agreement was also found for other values of K_1, K_2, and K_w. We must also mention that the theoretically predicted scaling property of the main peaks of the concentration profiles just illustrated in Fig. 5(b), also appears in the simulation results. For example, if the simulations results corresponding to the systems already presented in Fig. 5 are displaced following the same procedure as in Fig. 5 for the theoretical curves, the main peaks of the simulation results corresponding to each

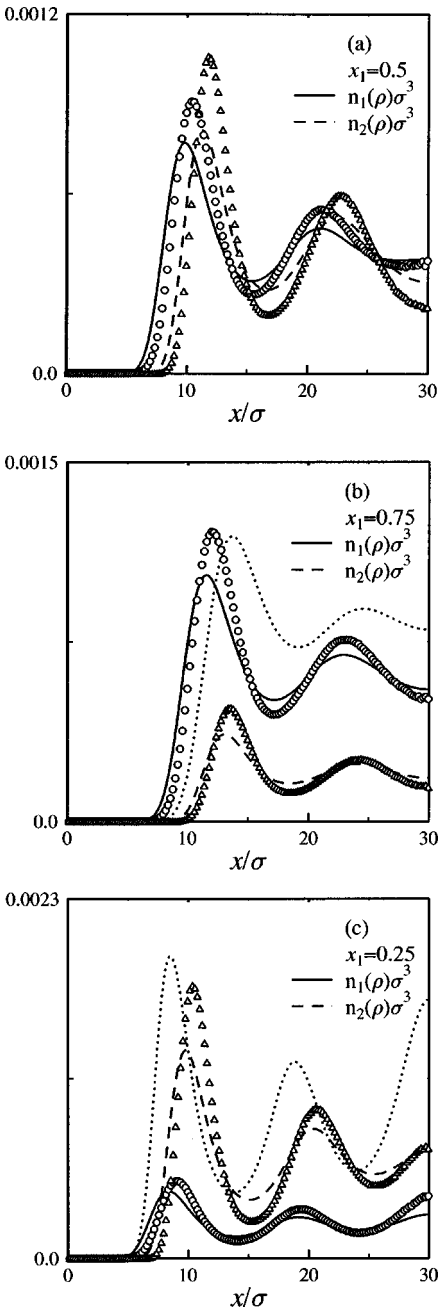

FIG. 6. (a) Comparison between theoretical results and simulation for the molar fraction $x_1=0.5$. Circles correspond to the simulated $n_1^*(\rho)$, whereas triangles correspond to the simulated $n_2^*(\rho)$. The parameters of the system are the same as in Fig. 5 for the case of $K_w=10$. The predicted results for the mean concentration of particles inside the cylinder are $\overline{n_1^*}=2.69\times10^{-4}$ and $\overline{n_2^*}=2.32\times10^{-4}$. (b) Comparison between theoretical results and simulation for the molar fraction $x_1=0.75$ and for the same parameters as in the previous figure. The predicted values for the mean concentration of particles inside the cylinder are $\overline{n_1^*}=3.45\times10^{-4}$ and $\overline{n_2^*}=9.82\times10^{-5}$. Symbols are as in (a). The dotted curve corresponds to the concentration profile of species 1 in the monodisperse limit $x_1=1$. (c) Comparison between theoretical results and simulation for the molar fraction $x_1=0.25$ and for the same parameters as in (a). The predicted values for the mean concentration of particles inside the cylinder are $\overline{n_1^*}=1.52\times10^{-4}$ and $\overline{n_2^*}=3.95\times10^{-4}$. Symbols are as in (a). The dotted curve corresponds to the concentration profile of species 2 in the monodisperse limit $x_2=1$ $(x_1=0)$.

species will superimpose. We see from these comparisons that the simulations confirm the general trends predicted by the theory, although the agreement is not perfect. Such disagreement we believe is mainly due to the approximations involved in deriving and solving Eq. (2.6). The most important of these approximations is the replacement of the inhomogeneous direct correlation function $c_{ij}(\mathbf{r},\mathbf{r}')$ by its homogeneous counterpart $c_{ij}^b(r)$. Another approximation is the use of approximate closure relations to close the set of equations given in Eq. (2.4).

So far we have presented the behavior of the structure for the case of equimolar mixtures. However, another relevant parameter determining the structure of the mixture inside the cylinder is the molar composition since, depending on the bulk composition of the mixture, the structure might be dominated by one of the species. Thus, our aim now is to present the comparison between theoretical and simulation results for nonequimolar mixtures, and to discuss the extent to which the structural order of the suspension depends on the bulk composition. For this, and still in the regime of narrow cylinders $(R'=30\sigma)$, we present the results of our theory when varying the composition of the mixture, along with their simulation counterparts. This is done in Figs. 6(b) and 6(c), where both theoretical and simulated concentration profiles for a system with the same parameters as in Fig. 6(a) are presented, but now for two different values of the molar fraction of species 1 ($x_1=0.25$, and 0.75). The theoretically predicted values for the mean concentration $\overline{n_1^*}$ and $\overline{n_2^*}$ of particles inside the cylinder for the case $x_1=0.25$ are $\overline{n_1^*}=1.52\times10^{-4}$ and $\overline{n_2^*}=3.95\times10^{-4}$, whereas for the case $x_1=0.75$ are $\overline{n_1^*}=3.45\times10^{-4}$ and $\overline{n_2^*}=9.82\times10^{-5}$. From these predicted values for $\overline{n_1^*}$ and $\overline{n_2^*}$ we see that through the process of increasing x_1 the mean concentration $\overline{n_1^*}$ of species 1 increases, whereas the mean concentration $\overline{n_2^*}$ decreases, but the ratio $\overline{n_1^*}/\overline{n_2^*}$ is not the same as the ratio n_1/n_2 of the bulk concentrations.

In Fig. 6(b) we have also plotted the concentration profile $n_1^*(\rho)$ for the limiting case $x_1=1$ (dotted curve), whereas in Fig. 6(c) the dotted curve corresponds to the concentration profile $n_2^*(\rho)$ for the limiting case $x_1=0$ (i.e., $x_2=1$). Notice that the curve corresponding to the monodisperse limit of species 1 has a larger gap near the wall (i.e., the suspension is more confined), and the amplitude of its oscillations is much weaker, than those of the curve corresponding to the monodisperse limit of species 2. Thus, from the comparison between these dotted curves we clearly see that the monodisperse limit of species 2 is much more structured than the monodisperse limit of species 1. With these monodisperse limits as reference systems, we better appreciate the effects induced by the variation of the molar composition of the mixture. For instance, starting with a monodisperse system of particles of species 1 [dotted curve in Fig. 6(b)], and ending with a monodisperse system of species 2 [dotted curve in Fig. 6(c)], we see that the substitution of particles of species 1 by particles of species 2 (i.e., decreasing x_1) displaces the concentration profiles to the left (towards the wall) and an additional peak centered in $\rho=0$ appears. This means that the system becomes more structured as the concentration of the more charged particles increases. During this process the

average repulsive particle-particle interaction energy per particle also increases, forcing the depletion gaps to decrease. By comparing $n_2^*(\rho)$ from Fig. 6(b) with $n_1^*(\rho)$ from Fig. 6(c) we see that the particles of species 1 are more structured than particles of species 2, since $n_1^*(\rho)$ has three peaks and a depletion gap of about 6σ, whereas $n_2^*(\rho)$ has two peaks and a depletion gap of about 10σ. In Fig. 6(c) $n_1^*(\rho)$ is so structured because particles of species 1 are immersed in a medium mainly constituted by particles of species 2 ($x_2 = 0.75$), which induce stronger correlations. On the other hand, for the case presented in Fig. 6(b), particles of species 2 are immersed in a medium mainly constituted by particles of species 1 ($x_1 = 0.75$), which makes the correlations weaker than in the case $x_2 = 0.75$. Thus we can state that species 2 highly emphasizes the structure of species 1, whereas the abundance of species 1 tends to weaken the structure of species 2. It is important to notice that the discussion above holds for both theory and simulations. Thus, at least qualitatively, and also quantitatively to the extent illustrated by the figures, we can say that the simulation results confirm all the general trends that the theory had predicted.

IV. SUMMARY

In this work we have presented a study of the structure of a model colloidal mixture consisting of highly charged colloidal particles confined in the interior of a highly charged cylinder. For such a study we have employed a simple theoretical approach that allows the determination of the concentration profiles once the interaction potentials and the bulk correlation functions $c_{ij}^b(r)$ are given. For the particle-particle interactions we took the repulsive part of the DLVO pair potential, whereas for the wall-particle interactions we adopted a functional form that derives from a Debye-Hückel description of such interactions [7]. The study of the structure was focused on two different regimes, namely, thick and narrow cylinders, where we have studied the effects of varying the size and charge of the pore, as well as the effects induced by variations in the bulk composition of the mixture.

Since from the beginning we restricted our study to large values in K_w, the first general feature of the concentration profiles is the appearance of a region near the wall where particles are not allowed to be in. These depletion gaps are found to be larger for the more charged species. Already in the regime of thick cylinders, which is defined by the condition $R_{\mathrm{ef}} \gtrsim \lambda$, it was found that the width of the depletion gaps depends only on the parameter K_w. In this same regime it was observed that there is a threshold value for R' above which we can safely refer to the regime of *very* thick cylinders. This regime is characterized by the appearance of bulk-like regions in the middle of the cylinder. When this happens, the shape of the concentration profiles $n_1^*(\rho)$ and $n_2^*(\rho)$ is found to be independent of both R' and K_w. Such scaling properties derive as a consequence of the asymptotic behavior of the wall-particle interaction potential $\Psi_i(\rho)$ ($i = 1,2$), which becomes independent of R' in the limit $R' \to \infty$. By reducing the size of the cylinder we arrive at the regime of narrow cylinders ($R_{\mathrm{ef}} \lesssim \lambda$). Here we focussed on the behavior of the structure as the wall-particle interaction is increased. During this process, an approximate scaling property for the main peaks of the concentration profiles $n_1^*(\rho)$ and $n_2^*(\rho)$ shows up, consisting of an invariance in the shape of these peaks under variations of the wall-particle interactions. This feature is a clear reminiscence of a scaling property of our model system that holds exactly in the limit of infinitely thick cylinders [6]. Another parameter that was investigated in this work was the bulk molar fraction. It turned out that the concentration profiles are very sensitive to variations in this parameter, and that the bulk density of one of the species has important effects on the structure of the other species. Finally, the theoretical results were compared with computer simulations for some of the systems studied, and it was found that the theoretical results follow quite well, although mostly semiquantitatively, the general trends shown by the simulations for both equimolar and nonequimolar, mixtures. In fact, in the case of equimolar mixtures we showed that the scaling property discussed and observed in the theoretically predicted results for $n_1^*(\rho)$ and $n_2^*(\rho)$ were also confirmed by our simulations.

ACKNOWLEDGMENTS

The authors wish to thank Dr. J. M. Méndez-Alcaraz for providing the program to calculate the Rogers-Young's bulk direct correlation function. We also thank the Computer Center of the Universidad de Guadalajara, Mexico, where some calculations were made. This work was partially supported by the Consejo Nacional de Ciencia y Tecnología (CONACyT, México) through Grant No. 2882E.

[1] E. J. W. Verwey and J. T. G. Overbeek, *Theory of the Stability of Lyophobic Colloids* (Elsevier, Amsterdam, 1948); M. Medina-Noyola and D. A. McQuarrie, J. Chem. Phys. **73**, 6279 (1980).

[2] D. H. van Winkle and C. A. Murray, J. Chem. Phys. **89**, 3885 (1988).

[3] M. D. Carbajal-Tinoco, F. Castro-Román, and J. L. Arauz-Lara, Phys. Rev. E **53**, 3745 (1996); G. M. Kepler and S. Fraden, Phys. Rev. Lett. **73**, 356 (1994); J. C. Crocker and D. G. Grier, *ibid.* **73**, 352 (1994).

[4] P. González-Mozuelos, J. Chem. Phys. **98**, 5747 (1993).

[5] P. González-Mozuelos and J. Alejandre, J. Chem. Phys. **105**, 5949 (1996).

[6] P. González-Mozuelos, J. Alejandre, and M. Medina-Noyola, J. Chem. Phys. **97**, 8712 (1992).

[7] M. Chávez-Páez, H. Acuña-Campa, L. Yeomas-Reyna, M. Valdez-Covarrubias, and M. Medina-Noyola, Phys. Rev. E **55**, 4406 (1997).

[8] G. Arfken, *Métodos Matemáticos Para Físicos* (Editorial DIANA, México, 1981)

[9] P. González-Mozuelos, J. Alejandre, and M. Medina-Noyola, J. Chem. Phys. **95**, 8337 (1991).

[10] F. J. Rogers and D. A. Young, Phys. Rev. A **30**, 999 (1984).

[11] R. Krause, B. D'Aguanno, J. M. Méndez-Alcaraz, G. Nägle, R. Klein, and R. Weber, J. Phys.: Condens. Matter **3**, 4459 (1991); J. M. Méndez-Alcaraz, B. D'Aguanno, and R. Klein, Physica A **178**, 421 (1991); Langmuir **8**, 2913 (1992).

[12] M. P. Allen and D. J. Tildesley, *Computer Simulation of Liquids* (Clarendon Press, Oxford, 1987).

[13] D. L. Ermak and J. A. McCammon, J. Chem. Phys. **69**, 1352 (1978).